

## **Ultrafast ferromagnetic spin switching by a single pair of optical pulses**

YAMADA, Kihiro T, RUTA, Sergiu <<http://orcid.org/0000-0001-8665-6817>>, KIMEL, Alexey V, PRABHAKARA, Kiran Horabail, LI, Tian, ANDO, Fuyuki, SEMIN, Sergey, ONO, Teruo, KIRILYUK, Andrei, CHANTRELL, Roy W and RASING, Theo

Available from Sheffield Hallam University Research Archive (SHURA) at:

<https://shura.shu.ac.uk/35730/>

---

This document is the Accepted Version [AM]

**Citation:**

YAMADA, Kihiro T, RUTA, Sergiu, KIMEL, Alexey V, PRABHAKARA, Kiran Horabail, LI, Tian, ANDO, Fuyuki, SEMIN, Sergey, ONO, Teruo, KIRILYUK, Andrei, CHANTRELL, Roy W and RASING, Theo (2025). Ultrafast ferromagnetic spin switching by a single pair of optical pulses. IEEE Transactions on Magnetics. [Article]

---

**Copyright and re-use policy**

See <http://shura.shu.ac.uk/information.html>

# Ultrafast ferromagnetic spin switching by a single pair of optical pulses

Kihiro T. Yamada<sup>1,6,\*</sup>, Sergiu Ruta<sup>2,7,\*</sup>, Alexey V. Kimmel<sup>1</sup>, Kiran Horabail Prabhakara<sup>1</sup>, Tian Li<sup>3</sup>, Fuyuki Ando<sup>3</sup>, Sergey Semin<sup>1</sup>, Teruo Ono<sup>3,4</sup>, Andrei Kirilyuk<sup>5</sup>, Roy W. Chantrell<sup>2</sup>, *Fellow, IEEE* and Theo Rasing<sup>1</sup>, *Member, IEEE*

<sup>1</sup> Radboud University, Institute for Molecules and Materials, Nijmegen 6525 AJ, The Netherlands.

<sup>2</sup>Department of Physics, University of York, Heslington, York YO10 5DD, United Kingdom.

<sup>3</sup>Institute for Chemical Research, Kyoto University, Uji 611-0011, Japan.

<sup>4</sup>Center for Spintronics Research Network, Institute for Chemical Research, Kyoto University, Uji 560-8531, Japan.

<sup>5</sup>FELIX Laboratory, Radboud University, Nijmegen 6525 ED, The Netherlands.

<sup>6</sup>Present address: Department of Physics, Institute of Science Tokyo, Tokyo 152-8551, Japan

<sup>7</sup>Present address: College of Business, Technology and Engineering, Sheffield Hallam University, United Kingdom

\*Corresponding authors: yamada.k.9463@m.isct.ac.jp; sergiu.ruta@shu.ac.uk

**All-optical magnetic recording potentially realizes orders of magnitude faster and more energy-efficient writing of magnetic bits but all-optical switching of ferromagnets is so far ultraslow. Here, we demonstrate a new mechanism to all-optically switch ferromagnetic spins on picosecond time scales by using a pair of one femtosecond (fs) linearly polarized ( $\pi$ ) and one properly-delayed picosecond (ps) circularly polarized ( $\sigma$ ) laser pulse for a Pt/Co/Pt multilayer. Our experiments show that the helicity dependent absorption of the ps-delayed  $\sigma$  pulse can deterministically steer the spin relaxation after destroying the ferromagnetic order by the fs  $\pi$  pulse. Atomistic spin-dynamics simulations show that the reversal occurs within approximately 3 ps through an unprecedented mechanism, where nanoscale spin textures created by the fs  $\pi$  pulse preferentially switch via magnetic circular dichroism, producing a spin- and helicity-dependent temperature difference of only a few Kelvin. Thus, a new route to deterministic ultrafast switching of nanoscale ferromagnetic media for ultra-high-density recording is opened up.**

*Index Terms*— ultrafast magnetization reversal, all-optical helicity-dependent switching, All Optical switching/recording.

## I. INTRODUCTION

For ferromagnets, where all the spins are parallel aligned by the exchange interaction, one can coherently switch the spin directions by an external force, e.g., a magnetic field, spin torques, [2,3 electric field [4,5], etc. This coherent spin switching has been the writing principle of magnetic recording devices, such as magnetic hard-disc drives[6,7] and magnetic random-access memories.[8] For such magnetic memories employing ferromagnets, the switching time is sub-nanosecond at the very least [9,10] due to the inductive technologies required to generate the switching field. To reduce the switching time of ferromagnets to picosecond time scales, an impractically large external force is necessary,[11–14] which has shifted the attention of scientific communities to ferrimagnets[15] and antiferromagnets[16,17] where the spin orientation can be switched in picoseconds. However, ferromagnets remain technologically crucial, because of their high anisotropy and relative ease of production, and considering the accumulated core technologies of magnetic devices. Therefore, it would be a breakthrough to discover a route to deterministically switch ferromagnetically-coupled spins on a picosecond time scale by a small external force.

The use of a strong nonequilibrium state[18,19] created by a femtosecond (fs) laser pulse might be an effective route for ultrafast magnetization reversal of a ferromagnetic metal by a small driving force. Thin ferrimagnetic GdFeCo films[20–24] exhibit magnetization reversal within 1 ps driven by a laser-induced strong nonequilibrium,[21] where the spin angular momenta of the Gd magnetic sublattice are transferred to the completely demagnetized Fe and Co sublattices through the exchange interactions during its ultrafast demagnetization[25].

Furthermore, spin currents arising during the demagnetization of the ferrimagnetic film can be used to switch an adjacent ferromagnetic film. In contrast to the helicity-independence of these all-optical phenomena, all-optical switching (AOS) in thin ferromagnetic metals, such as Co/Pt multilayers[28–35] and FePt granular media,[28,36,37] depends advantageously on the light helicity but is incomparably slow. This is because the all-optical helicity-dependent switching (AO-HDS) proceeds via a two-step process[29], that starts with a helicity-independent formation of switched domains while being completed via slow domain wall displacements by multiple circularly polarized pulses via magnetic circular dichroism (MCD) [38–40]. Note that, using a hundred fs pulses of an amplified laser with a 1 kHz repetition rate takes 0.1 second. The inefficiency of the conventional AO-HDS in these systems results from the fact that the circularly polarized pulses act on equilibrium and thus stable magnetic domains.

Here, we demonstrate that dual-pulse AO-HDS[41] proceeds via an unprecedented ultrafast process driven by a small

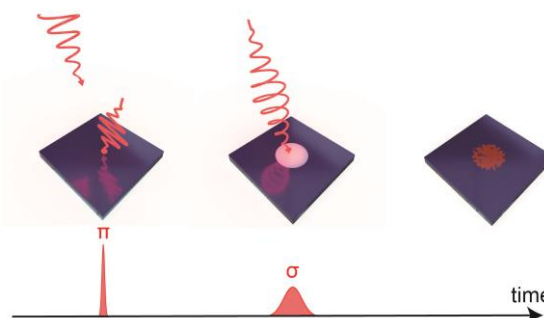


Fig. 1. Principal concept of dual-pulse all-optical helicity dependent switching (AO-HDS).

external force. As conceptually shown in Fig. 1, a first fs linearly polarized laser pulse destroys the macroscopic spin order of a Pt/Co/Pt multilayer and creates nonequilibrium nanoscale nuclei of correlated spins. After a separation time  $\Delta t$ , a second ps circularly polarized pulse deterministically steers the nonequilibrium nanoscale nuclei to either uniformly up- or down-magnetized state by a small helicity-dependent laser absorption. At  $\Delta t = 5$  ps, a single pulse pair deterministically switched approximately 80 percent of spins inside the illuminated area. The dual-pulse AO-HDS was optimized within a narrow window centered around  $\Delta t = 5$  ps. Time-resolved magneto-optical measurements on the dynamics triggered by a pulse pair show that the ps  $\sigma$  pulse controls the ps spin relaxation in a helicity-dependent way, after ultrafast demagnetization by the fs  $\pi$  pulse. Our atomistic spin-dynamics simulations of the dual-pulse AO-HDS reproduce the narrow optimal window of  $\Delta t$  for the spin switching. The time evolution of the mapped electron and spin temperature enables us to conclude that the nonequilibrium spin textures created by the fs  $\pi$  pulse reverse within about 3 ps by the spin- and helicity-dependent temperature difference of only a few Kelvin produced by the ps  $\sigma$  pulse, a mechanism circumventing the need for domain wall displacement and, importantly, operating at the nanoscale. Thus, this dual-pulse approach brings deterministic AO-HDS of ferromagnets to the sub-THz regime, i.e., a  $10^6$  to  $10^9$  times faster than possible using domain wall processes.

## II. EXPERIMENTAL METHODS

*Sample preparations:* The multilayer of Ta (4 nm)/Pt (3.0 nm)/Co (0.8 nm)/Pt (3.0 nm)/MgO (2.0 nm)/Ta (1.0 nm) was sputtered on a synthetic quartz glass substrate. DC and RF sources were used for depositing Ta, Pt, and Co, and MgO, respectively. The MgO/Ta capping layer prevents the magnetic layer from oxidization. The multilayer exhibits a perpendicular easy axis of magnetization. The effective magnetic anisotropy field and constant are 1.16 T and  $9.4 \times 10^5$  J/m<sup>3</sup>, respectively, with a typical saturation magnetization of  $1.6 \times 10^6$  A/m. Using these magnetic parameters, the exchange stiffness constant was estimated to be  $9.8 \times 10^{-12}$  J/m from the equilibrium domain width (14.5  $\mu$ m) [49].

*Magneto-optical imaging:* For optical excitation, we used a Ti: sapphire amplified laser system (Solstice Ace, Spectra-Physics) of which the central wavelength and repetition rate were 800 nm and 1 kHz, respectively. The amplifier system contains two compressors which allowed independent control of the pulse width for the two pump beams. The laser amplifier was used in external trigger mode, in which, with the help of a delay generator (DG645, Stanford Research) we can control the number of pulses reaching the sample. Magneto-optical Faraday imaging with a white light source as probe was employed for detection, see Fig. S1(a) in supplementary materials. The duration of the first linearly polarized pump pulse was about 90 fs while the second, circularly polarized pump pulse, was 4.5 ps long and arrived after an adjustable pulse interval,  $\Delta t$ . The laser pulses had a Gaussian intensity distribution and both were incident at an angle of 15 deg. from the sample normal. The focused beam sizes ( $1/e^2$  radius) of the

$\pi$  and  $\sigma$  pump pulses were calculated with the Liu method [24,50] to be  $35.5 \pm 0.7$   $\mu$ m and  $42.9 \pm 0.4$   $\mu$ m, respectively. The laser fluence was calculated using the  $1/e^2$  radius, the repetition rate (1 kHz), and the average power measured with a power meter. We controlled the pump intensity by using a combination of a half-wave plate and a Gran-Taylor prism. To achieve precise intensity control of the circularly-polarized pump, the half-wave plate was mounted on a motorized stage. A quarter-wave plate was placed after the Gran-Taylor prism to convert the linearly polarized beam to a circularly polarized one for the second pump. The probe light from the white light source was linearly polarized by a sheet polarizer. It was then collimated and incident on the sample surface using a combination of lenses. The polarization of the incident probe light is rotated by the magneto-optical Faraday effect of the sample. The transmitted light from the sample was collected by an objective with a magnification of 20 $\times$ . The polarization rotation was analyzed by a Gran-Taylor prism, of which the polarization axis is almost orthogonal to the polarization of the incident probe light. Then, a charge-coupled device (CCD) camera behind the analyzer can visualize magnetic domains.

*Time-resolved magneto-optical measurements:* For the pump-probe measurements, the laser amplifier was operated in the internal trigger mode at 1 kHz. See Fig. S1(b) in supplementary materials for the schematic. An optical parametric amplifier (OPA) was used to tune the wavelength of the output from the internal compressor to 1000 nm. Moreover, the output from the OPA was separated into two beams. One was used as the first  $\pi$  pump pulse after the wavelength was converted to 500 nm by a beta-barium borate crystal. We put a delay line on the other beam, which was used as the probe beam. We used the output from the external compressor for the  $\sigma$  pulse as done in the static measurements. The repetition rates of the two pump pulses were brought down to 500 Hz by a mechanical chopper. After the intensity of the probe beam was weakened by a combination of a half-wave plate and a Gran-Taylor prism, the probe beam was incident onto the film surface. The transmitted light collected by the objective went through a long pass filter into a balanced detector to measure the Faraday rotation. While varying the delay line, we measured the perpendicular magnetization component through the Faraday effect at an arbitrary time before and after the pump pulses arrived at the sample. During the pump-probe measurements, we applied a magnetic field of 3.3 mT along the normal to the sample to set the initial magnetic state. The field was generated by two permanent magnets on either side of the sample. The  $1/e^2$  radii were  $31.6 \pm 0.7$   $\mu$ m,  $29.7 \pm 0.9$   $\mu$ m, and  $62.7 \pm 1.4$   $\mu$ m for the probe, the short  $\pi$  polarized, and the long  $\sigma$  beams, respectively. We fixed the fluence of the probe beam at 0.32 mJ/cm<sup>2</sup>, which was much smaller than those of the  $\pi$  and  $\sigma$  pump beams (2.31 mJ/cm<sup>2</sup> and 2.50 mJ/cm<sup>2</sup>, respectively).

## III. ATOMISTIC SPIN-DYNAMICS SIMULATIONS

For the numerical investigation of spin dynamics under femtosecond laser excitation, we developed an atomistic spin-

dynamics model of Co thin films. The energy of the system is described by the spin Hamiltonian:

$$\mathcal{H} = - \sum_{i < j} J_{i,j} \mathbf{S}_i \cdot \mathbf{S}_j - \sum_i k_u (\mathbf{S}_i^z)^2, \quad (1)$$

where the spin  $\mathbf{S}_i$  is a unit vector describing the local spin direction. It is normalized to the local atomic spin magnetic moment ( $\mu_{\text{Co}}$ ). We use  $\mu_{\text{Co}} = 1.61 \mu_{\text{B}}$  and nearest-neighbour Co-Co exchange of  $J = 4.8 \times 10^{-21} \text{ J}$ . The atomistic spin-dynamics model allows atomistic level resolution of spin dynamics, which is important in understanding small spin textures forming immediately after the laser excitation. The compromise is that the simulated systems are relatively small. In this case, we consider a  $25 \text{ nm} \times 25 \text{ nm} \times 10 \text{ nm}$  system with periodic boundary conditions in  $x$  and  $y$  directions (to mimic a thin film) or a  $8 \text{ nm} \times 8 \text{ nm} \times 10 \text{ nm}$  nanodot. To be able to capture multiple domain structures, the magnetic anisotropy  $k_u$ , was enhanced and taken  $5.85 \times 10^{-23} \text{ J}$ , one order of magnitude larger than reported in the literature by Moreno et al [51] such that the smallest stable domain is around 6 nm. The system dynamics are computed using the VAMPIRE software package [43] based on the Landau-Lifshitz-Gilbert (LLG) equation:

$$\frac{\partial \mathbf{S}_i}{\partial t} = - \frac{\gamma}{(1 + \alpha^2)} [\mathbf{S}_i \times \mathbf{B}_{\text{eff}}^i + \alpha_i \mathbf{S}_i \times (\mathbf{S}_i \times \mathbf{B}_{\text{eff}}^i)], \quad (2)$$

where  $\gamma$  is the gyromagnetic ratio of  $1.76 \times 10^{11} \text{ T}^{-1} \text{ s}^{-1}$  and  $\alpha$  is the Gilbert damping factor of 0.10. The on-site effective field can be computed as the summation of the local field derived from the spin Hamiltonian with a random field to model the heat bath:

$$\mathbf{B}_{\text{eff}}^i = - \frac{\partial \mathcal{H}}{\partial \mathbf{S}_i} + \boldsymbol{\zeta}_i, \quad (3)$$

where  $\boldsymbol{\zeta}_i$  is a stochastic thermal field due to the interaction of the conduction electrons with the local spins. The stochastic thermal field is assumed to have Gaussian statistics and satisfies:

$$\begin{aligned} \langle \zeta_{i,a}(t) \zeta_{j,b}(t') \rangle &= \delta_{ij} \delta_{ab} (t - t') 2\alpha_i k_B T / \gamma_i \mu_i, \\ \langle \zeta_{i,a}(t) \rangle &= 0, \end{aligned} \quad (4)$$

where  $a, b$  are Cartesian components;  $k_B$  is the Boltzmann constant and  $T$  is the temperature. We incorporate the rapid change in the thermal energy of a system under the influence of a femtosecond laser pulse. The spin system is coupled to the electron temperature,  $T_e$ , which is calculated using the two-temperature model [52]:

$$T_e \gamma_e \frac{dT_e}{dt} = -G_{\text{el}}(T_1 - T_e) + P(t), \quad (5)$$

$$C_1 \frac{dT_1}{dt} = -G_{\text{el}}(T_e - T_1), \quad (6)$$

where  $\gamma_e = 700 \text{ Jm}^{-3} \text{ K}^{-2}$ ,  $C_1 = 3.0 \times 10^6 \text{ Jm}^{-3} \text{ K}^{-1}$ , and  $G_{\text{el}} = 6.0 \times 10^{17} \text{ Wm}^{-3} \text{ K}^{-1}$ .  $P(t)$  models the temperature from the laser pulse into the electronic system. Here, we consider a combination of two pulses: a first linearly polarized pulse and a second circularly polarized pulse,

$$P(t) = P_1(t) + (1 + f_{\text{MCD}}(s_z)) g_{\text{MCD}}(T) P_2(t), \quad (7)$$

where  $f_{\text{MCD}}(s_z)$  is assumed in first approximation to be a linear function between MCD for  $s_z = +1$  and the -MCD value for  $s_z = -1$ . The MCD effect is included as linearly dependent on the  $z$  component of the atomic site spin moment. Also, we consider that the strength of the MCD effect is proportional to

the temperature. At high temperatures, due to the disordered nature of the spins and the electronic structure, the MCD needs to decrease to zero. To incorporate this effect, we model the temperature dependence of the MCD as:

$$g_{\text{MCD}}(T) = g_{\text{MCD}}(T = 0 \text{ K}) (1 - T/T_C)^{0.33}. \quad (8)$$

We used the MCD parameter  $g_{\text{MCD}}(T = 0 \text{ K}) = 0.02$  and the Curie temperature  $T_C = 1110 \text{ K}$ . There is no expected MCD effect when the system is completely disordered just 10K below the Curie temperature of the magnetic system. The two-temperature model needs to be solved for each atomic site ' $i$ ':

$$T_e^i C_e \frac{dT_e^i}{dt} = -G_{\text{el}}(T_1 - T_e^i) + P^i(t, s_z^i) - \frac{(T_e^i - \langle T_e \rangle)}{\tau_{\text{el}}}, \quad (9)$$

$$C_1 \frac{dT_1}{dt} = -G_{\text{el}}(\langle T_e \rangle - T_1), \quad (10)$$

$$\langle T_e \rangle = \frac{1}{N} \sum (T_e^i), \quad (11)$$

, where  $\tau_{\text{el}} = 0.10 \text{ ps}$ . In a first approximation, we can simplify this equation as:

$$T_e^{s_z=+1} \gamma_e \frac{dT_e^{s_z=+1}}{dt} = -G_{\text{el}}(T_1 - T_e^{s_z=+1}) + P(t, s_z = +1) - \frac{T_e^{s_z=+1} - \langle T_e \rangle}{\tau_{\text{el}}}, \quad (12)$$

$$T_e^{s_z=-1} \gamma_e \frac{dT_e^{s_z=-1}}{dt} = -G_{\text{el}}(T_1 - T_e^{s_z=-1}) + P(t, s_z = -1) - \frac{T_e^{s_z=-1} - \langle T_e \rangle}{\tau_{\text{el}}}. \quad (13)$$

In this way, we compute an electron temperature for a system magnetized in either  $+z$  or  $-z$  direction and the electronic temperature for each spin (atomic site) is computed by interpolation:

$$T_e^i = \frac{(T_e^{s_z=+1} - T_e^{s_z=-1}) s_z + (T_e^{s_z=+1} + T_e^{s_z=-1})}{2}. \quad (14)$$

## IV. RESULTS

### A. Comparison between multi-pulse and dual-pulse AO-HDS

We prepared a Ta (4 nm)/Pt (3.0 nm)/Co (0.8 nm)/Pt (3.0 nm)/MgO (2.0 nm)/Ta (1.0 nm) on a synthetic quartz glass substrate by magnetron sputtering. Pt/Co/Pt systems are typical candidates for AO-HDS.[28–35,41] To characterize the switching in the studied structure, we first measured the switching by only  $\sigma$  polarized pulses in transmission geometry (see Methods sections for more details of the static magneto-optical measurements). Here, we used ps  $\sigma$  pulses that are more favorable for the AO-HDS than fs  $\sigma$  pulses (see Ref. [31] and Fig. S2(a) and 2(b). Fig. 2(a) shows magneto-optical images taken after the Pt/Co/Pt film was excited with a sequence of 4.5-ps right( $\sigma^+$ )-handed or left( $\sigma^-$ )-handed circularly polarized light pulses. The electric field vectors of  $\sigma^+$  and  $\sigma^-$  light projected to a screen rotate clockwise and anticlockwise, respectively, when standing against the light source. The images were taken long after the excitation when the magnetization had already reached a stable state. The interval between the pulses was set to be at least 2 seconds. To fully switch the magnetization in the area with a diameter of 15- $\mu\text{m}$ , the experiments required 120-140 pulses.

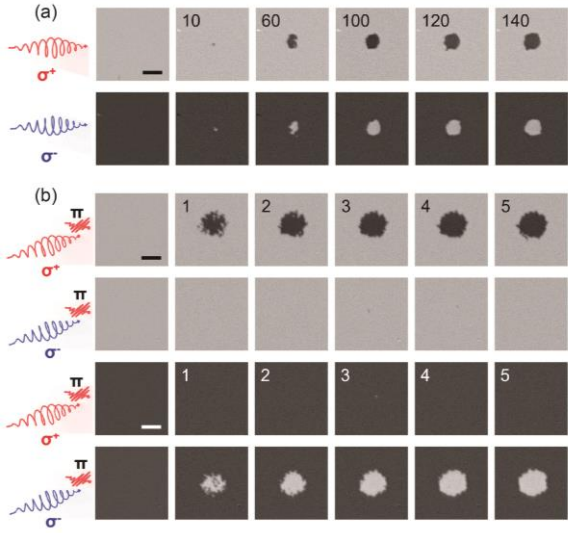


Fig. 2. Dual-pulse all-optical helicity dependent switching (AO-HDS). (a) AO-HDS by multiple right ( $\sigma^+$ ) and left ( $\sigma^-$ ) circularly polarized pulses. Here, the fluence of the 4.5-ps  $\sigma$  pulse was fixed at  $F_\sigma = 4.87 \text{ mJ/cm}^2$ . (b) Dual-pulse AO-HDS for a time separation  $\Delta t$  of 5.0 ps. Here, we used the fluence of  $F_\pi = 2.32 \text{ mJ/cm}^2$  for the 90-fs  $\pi$  pulse and  $F_\sigma = 2.37 \text{ mJ/cm}^2$ . The number of pulses (pairs) is indicated on each magneto-optical image. The darker and brighter areas denote up( $M^\uparrow$ )-magnetized and down( $M^\downarrow$ )-magnetized states, respectively. The scale bars correspond to 20  $\mu\text{m}$ .

Similar experiments with a pair of pulses show that the duration of the laser excitation required for the switching can be reduced dramatically. Fig. 2(b) shows the results of an experiment, in which the same Pt/Co/Pt stack was excited with one 90-fs  $\pi$  and one 4.5-ps  $\sigma$  pulse, separated by  $\Delta t = 5.0 \text{ ps}$ . Notably, a single pair of these pulses can switch a substantial (>80%) part of the same 15- $\mu\text{m}$  area in a helicity-dependent and deterministic way. In the case of excitation without  $\pi$  pulses, that is, with  $\sigma$  pulses only, a similar result would require more than 100 pulses [Fig. 2(a)].

### B. Time-separation dependence of dual-pulse AO-HDS

To find the optimal condition of the pulse pair for the switching, we measured magneto-optical images varying  $\Delta t$  of the pair [Fig. 3(a)]. The averaged net magnetization  $\langle M \rangle$  after illumination with a pulse pair as a function of  $\Delta t$  is shown in Fig. 3(b).  $\langle M \rangle$  was determined by averaging the intensities of all the pixels in the 15- $\mu\text{m}$ -area, normalized to the average intensity of the image for a uniformly magnetized sample. Fig. 3(c) shows the helicity-dependent switching efficiency, which is defined as  $\langle M \rangle [(M^\uparrow, \sigma^+) - (M^\downarrow, \sigma^-) - (M^\uparrow, \sigma^-) + (M^\downarrow, \sigma^+)] / 4$ , as a function of  $\Delta t$ . Here, ( $M^\uparrow, \sigma^+$ ) means that the magnetic state was originally saturated in the up direction and the ps pulse was right-handed circularly polarized. The optimal switching is observed when the ps  $\sigma$  pulse arrives around 5.0 ps after the fs  $\pi$  pulse. Longer separation reduces the switching efficiency dramatically. No switching and only demagnetization is observed if the fs  $\pi$  pulse arrives after the ps  $\sigma$  pulse, because the fs  $\pi$  pulse breaks any helicity-

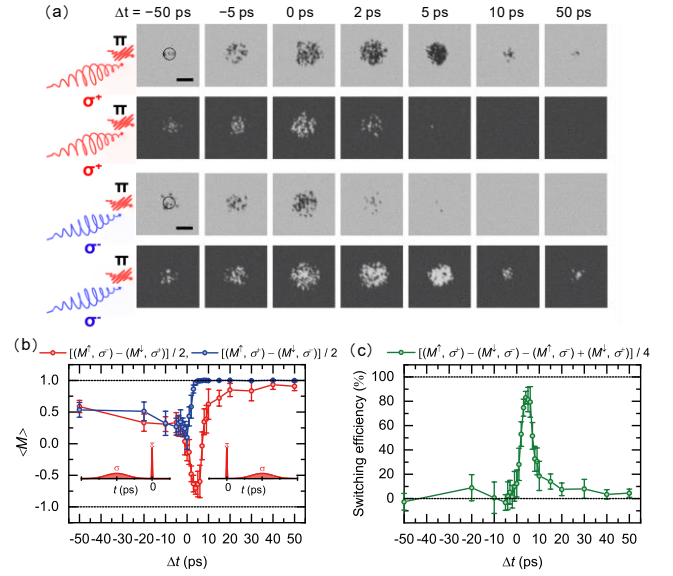


Fig. 3. Time-separation ( $\Delta t$ ) dependence of the AO-HDS. (a) Magneto-optical images after the excitation of a pulse pair for various  $\Delta t$ . The laser parameters were the same as in Fig. 1c. The scale bars correspond to 20  $\mu\text{m}$ . A 15- $\mu\text{m}$  diameter area for integration is indicated by a solid-line circle. b, c) Average net magnetization  $\langle M \rangle$  (b) and switching efficiency (c) after the illumination of a pulse pair as a function of  $\Delta t$ . We defined the switching efficiency as  $\langle M \rangle [(M^\uparrow, \sigma^+) - (M^\downarrow, \sigma^-) - (M^\uparrow, \sigma^-) + (M^\downarrow, \sigma^+)] / 4$ . Here, ( $M^\uparrow, \sigma^+$ ) means that a right circularly polarized pulse was given to the up-magnetized background. As shown in the insets of Fig. 2(b), positive (negative)  $\Delta t$  means that the long  $\sigma$  pulse reaches the sample later (earlier) than the short  $\pi$  pulse. The error bars were determined by repeating the same measurements five times.

dependent effect by heating the system above the Curie temperature. This result is in contrast to a previous dual-pulse experiment on GdFeCo with a similar combination of fs  $\pi$  and  $\sigma$  pulses [42], where the deterministic AOS is possible even for negative  $\Delta t$ . This difference is due to the fact that the AOS of GdFeCo is driven by heating the system to the Curie temperature regardless of the light helicity [22-24].

### C. Time-resolved measurement of dual-pulse AO-HDS

To reveal the ultrafast dynamics of the helicity-dependent switching with a pulse pair, we performed stroboscopic experiments (See Materials and Methods for more details of the time-resolved experiment) with sub-picosecond resolution. We excited the sample with a sequence of the pairs and measured the magnetization dynamics integrated over the excited area with the help of the magneto-optical Faraday effect. Fig. 4(a) reveals sub-10 ps dynamics triggered by the pair of  $\pi$  and  $\sigma$  pulses, measured for two helicities of the  $\sigma$  pulse.

Here, we applied a magnetic field of 33 mT to initialize the magnetization. The fs  $\pi$  pulse brings the medium into a nearly demagnetized state. The ps  $\sigma$  pulse steers the subsequent relaxation on a time scale of 5 ps in a helicity-dependent way. A much smaller helicity dependence is observed in

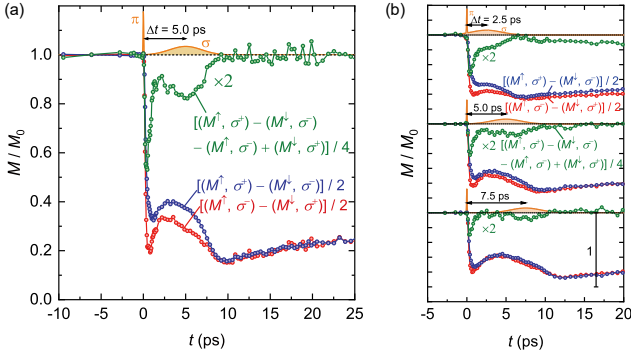


Fig. 4. Time-resolved magneto-optical measurements of the spin dynamics excited by a pulse pair. a) The normalized magnetization  $M / M_0$  as a function of delay time  $t$  for  $\Delta t = 5.0$  ps with the dual-pulse excitation. Here, we used  $F_\pi = 2.31$  mJ/cm<sup>2</sup> and  $F_\sigma = 2.50$  mJ/cm<sup>2</sup>. A magnetic field of 3.3 mT was applied to ensure that the magnetization relaxes back to the initial state. b) The time evolution of  $M / M_0$  and the difference for  $\Delta t = 2.5$  ps, 5.0 ps, and 7.5 ps. The Gaussian time profiles of the 90-fs  $\pi$  pulse and 4.5-ps  $\sigma$  pulse are also shown in the plots, where the peak heights were arbitrarily tuned for simplicity. The Pt/Co/Pt multilayer was permanently damaged for  $\Delta t = 0.0$  ps.

stroboscopic experiments with just ps  $\sigma$  pulses when the  $\pi$  pulses are blocked (see Fig. S3). The helicity-dependent effect on the magnetization dynamics disappears upon increasing  $\Delta t$  between the pulses from 2.5 ps to 7.5 ps (see Fig. 4(b)). The largest helicity dependent effect is observed particularly in the demagnetization peak for  $\Delta t = 2.5$  ps whereas  $\Delta t = 5.0$  ps is optimal in the static measurements [Fig. 3(c)]. With decreasing  $\Delta t$  to 0 ps, the nonequilibrium state should be more strongly affected by the ps  $\sigma$  pulse but the subsequent ps spin relaxation is exposed to larger thermal fluctuations, randomizing the spin directions. These larger thermal fluctuations during the spin relaxation may be why the final magnetization state is less well defined for the shorter separation. Note that, within 2.5–5.0 ps after the excitation with a fs pulse, the magnetic medium is still in a strongly nonequilibrium, nearly demagnetized state. The delay of 2.5–5.0 ps is within the ball-park of the characteristic times of the electron-phonon interaction in metals. Therefore, the experiments show that the  $\sigma$  pulse can deterministically steer the relaxation to one or another stable state in a helicity-dependent way only if the electron gas is out of equilibrium with the lattice.

#### D. Atomistic spin-dynamics simulation of dual-pulse AO-HDS

To understand the spatial-temporal aspects of this ultrafast switching dynamics, we have developed an atomistic spin-dynamics model [43] of the switching process. The model describes the production of randomly oriented nanometer-scale spin textures after ultrafast demagnetization due to the first 90 fs  $\pi$  pulse and the differential (helicity-dependent) heating of the spin textures by the second 4.5-ps  $\sigma$  pulse via

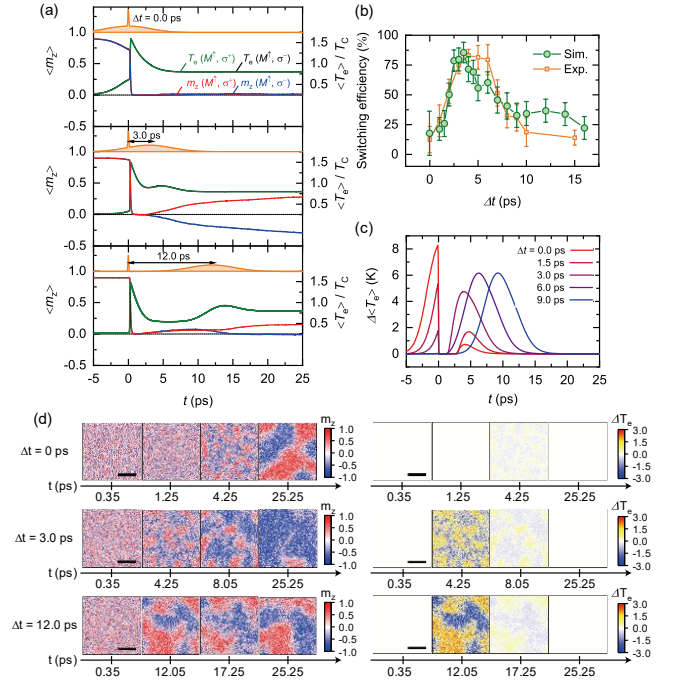


Fig. 5. Atomistic spin-dynamics simulation of the time-resolved magnetization dynamics. (a) The time evolution of the average  $z$  component of magnetization  $\langle m_z \rangle$  and average electron temperature  $\langle T_e \rangle$  per site for  $\Delta t = 0.0$  ps, 3.0 ps, and 12.0 ps. The  $T_e$  is normalized by the Curie temperature  $T_C = 1110$  K. Here, we fixed the magnetic circular dichroism (MCD) and the restoring magnetic field at 2.0 % and 3.0 mT, respectively. (b) The switching efficiency as a function of delay time ( $\Delta t$ ). The results indicate a switching efficiency around 90% for  $\sigma^-$  and a 10% for  $\sigma^+$  indicating a good control of the switching direction based on the light helicity. Because the temperature of the overall system at 35 ps is still high ( $T / T_C \sim 0.8$ ) at 35 ps, the average of  $m_z$  does not fully relax to the initial value (i.e.,  $\langle m_z \rangle = 1$ ). Therefore, we divided the simulated switching efficiency by a factor of 0.36 corresponding to an average value of  $\langle |m_z| \rangle$  at 35 ps. The same results from (b) are illustrated in the supplementary materials Fig. S6 using the experimental metrics of switching efficiency. (c) The temperature difference in  $\Delta T_e$  by the MCD between up and down spins as a function of  $t$ . (d) The time evolution of the mapped  $m_z$  and  $\Delta T_e$  for  $\Delta t = 0.0$  ps, 3.0 ps, and 12.0 ps illustrated for the larger system ( $25 \text{ nm} \times 25 \text{ nm} \times 10 \text{ nm}$ ). The scale bars correspond to 8 nm. See supporting movies for the detailed time evolutions of the  $m_z$  and  $\Delta T_e$  maps.

the mechanism of MCD. See Methods for more details of the simulations.

Fig. 5(a) shows the variations of the average magnetization  $\langle m_z \rangle$  and the average electronic temperature  $\langle T_e \rangle$  in the overall system with a size of  $25 \text{ nm} \times 25 \text{ nm} \times 10 \text{ nm}$  for  $\Delta t = 0.0$  ps, 3.0 ps, and 12.0 ps. We plot in Fig. 5(b) the  $\Delta t$  dependence of the switching efficiency,  $\langle m_z \rangle [(m_z^\uparrow, \sigma^+) - (m_z^\uparrow, \sigma^-)] / 2$ , where  $\langle m_z \rangle$  denotes the average net magnetization in a smaller system ( $8 \text{ nm} \times 8 \text{ nm} \times 10 \text{ nm}$ ) at 35 ps. We determined the average and standard error by 50 repetitions of the simulation. The switching efficiency has a

peak at  $\Delta t = 3.0$  ps in Fig. 5(b), which reproduces the peak feature observed in the experiments (see the inset of Fig. 3(c)). The switching efficiency is maximum (about 90%) at  $\Delta t = 3.0$  ps, indicating a good degree of control for deterministic switching. Given that the material and optical parameters are by no means optimized, this result shows promise for the use of dual-pulse switching for ultra-high density recording. Although we employed a small system, we obtained a similar peak in  $\langle m_z \rangle$  as a function of  $\Delta t$  as for the larger system (see Fig. S4). The time evolution of an electron-temperature difference  $\Delta \langle T_e \rangle$  by MCD in Fig. 5(c) clearly explains the reason for no spin switching at  $\Delta t = 0$  ps. Whereas the overlap between the two pulses ( $\Delta t = 0$  ps) produces the largest  $T_e$  [Fig. 5(a)], overheating the overall system above the Curie temperature  $T_C$  results in a large time interval, as long as 2.5 ps, during which the  $\Delta \langle T_e \rangle$  is zero [Fig. 5(c)]. Therefore, we find no spin switching and only thermal randomization for  $\Delta t = 0$  ps [Fig. 5(a)]. The switching efficiency increases as the time interval of  $\Delta \langle T_e \rangle = 0$  K decreases with increasing  $\Delta t$ . At the same time, the  $\Delta \langle T_e \rangle$  reaches a maximum value of around 4-6K after the initial demagnetization. This small temperature imbalance at the time of small spin texture being form is critical in providing control switching. The optimal  $\Delta t$  of 3.0 ps is slightly smaller than in the static experiment (5.0 ps) [Fig. 3(c)]. This difference suggests that, because the electron-phonon coupling predominantly determines the time interval of  $\Delta \langle T_e \rangle = 0$  K, the electron-phonon iso-thermalization in our Pt/Co/Pt sample is slower than in the simulations.

To inspect the switching dynamics, we furthermore mapped the  $m_z$  and  $T_e$  for  $\Delta t = 0.0$  ps, 3.0 ps, and 12.0 ps in Fig. 5(d) and the Supplementary Videos. The act of the fs  $\pi$  pulse destroys any macroscopic domain configurations to create nonequilibrium, small, and localized nanoscale magnetic textures [44]. The spin-reversal condition is defined not only by the amplitude of  $\Delta T_e$  but also by the size of the nonequilibrium spin textures. The simulated spin maps show that the spin textures are becoming larger and increasingly stable in time. Because too large spin textures cannot be switched by a small temperature difference, the switching efficiency decreases on increasing  $\Delta t$  beyond 3.0 ps. Thus, ultrafast and deterministic spin switching by a pair of  $\pi$  and  $\sigma$  pulses requires the preparation of nonequilibrium nanometer-size spin textures by a fs  $\pi$  pulse. Additionally, one must create a spin and helicity-dependent temperature difference of a few Kelvin by a ps  $\sigma$  pulse at the optimal timing, to avoid overheating the system above the Curie temperature. Unfortunately, we cannot observe nanoscale spin textures evolving on a picosecond time scale by our current optical experimental set-up. Time-resolved x-ray<sup>[44,45]</sup> and scanning-probe [46] techniques combined with a fs-laser system would be useful in the future to inspect this time- and length-scale spin dynamics.

## V. DISCUSSION

Ultrafast precessional spin switching by a ps magnetic field needs a magnetic field as large as several Tesla [11,12,14]. In contrast, the dual-pulse approach is advantageous in terms of magnetic-field amplitude for magnetization switching,

because switching laser-induced nonequilibrium spin textures only requires a small temperature difference of 6 K, which corresponds to a thermal random effective magnetic field of 20 mT within 5.0 ps. This sensitivity to an external magnetic field may explain the observation of no substantial difference in magnetization in Fig. 4(a) after the action of the ps  $\sigma$  pulse, even with a small restoring magnetic field of 3.3 mT. Increasing the magnetic field to 8.3 mT indeed suppresses the helicity-dependent effect on the ps spin relaxation by half (see Fig. S5) for  $\Delta t = 5.0$  ps.

Tudosa et al. [14] reported that the heating of a granular magnetic medium by a ps electron pulse determines the ultimate speed of the magnetization switching, because gigantic random torques from the exchange interaction between disordered spins extinguish the effect of the field torque. This situation may be similar to the case at  $\Delta t = 0$  ps, where the disordered spin and electronic structure limit the deterministic spin switching. Our experiments and simulations demonstrate that the speed limitation can be lifted if a ps  $\sigma$  pulse is exerted to the spins a few ps after the fs laser excitation.

The switching of the laser-induced nonequilibrium spin textures is  $10^6$ - $10^9$  times as fast as the conventional AO-HDS in ferromagnets, invariably requiring stable domains and domain wall expansions using hundreds of pulses that take milliseconds to seconds in total. The necessity of stable domains and the expansions means that the conventional AO-HDS is inapplicable to cutting-edge granular magnetic recording media [47], such as FePt [48] with single-magnetic domain grains of the order of ten nm. On the other hand, our dual-pulse approach can switch a nanometer single-magnetic domain within about 3 ps, as demonstrated by our atomistic spin-dynamics simulations of the smaller system (8 nm  $\times$  8 nm  $\times$  10 nm). Therefore, the dual-pulse approach breaks the rate as well as medium limitations to pave a pathway toward realizing the next-generation information-writing method that no longer requires an external magnetic field.

## VI. CONCLUSION

To summarize, we have demonstrated a novel approach using an optical pulse pair to bring magnetization switching of ferromagnetic Co/Pt to the ps regime. The switching is optimized by excitation with a pair of 90 fs  $\pi$  and 4.5 ps  $\sigma$  laser pulses, separated by about 5 ps. In this case, the first fs  $\pi$  laser pulse brings the medium into a strongly nonequilibrium, nearly demagnetized state. The second ps  $\sigma$  circularly polarized pulse affects a ps spin relaxation in a helicity-dependent way, which strongly depends on the time separation between the two pulses. Our results reveal that both ultrafast magnetization dynamics and the efficiency of the switching are most sensitive to the helicity of the  $\sigma$  pulse when the latter finds the sample in a strongly nonequilibrium state. The atomistic spin-dynamics simulations moreover unveil that nanometer-size nonequilibrium spin textures created by a fs  $\pi$  pulse are switched within about 3 ps, driven by a temperature difference of only a few Kelvin between up and down spins via MCD. The narrow spin-reversal window of the time separation is defined by the size of the nonequilibrium spin

textures and the strength of the MCD, which both depend on the system temperature evolving on a ps time scale. Manipulation of the magnetization on this time- and length-scale opens the possibility of new approaches to ultrafast spin dynamics and shows considerable promise for the switching of nanoscale ferromagnetic materials for future information storage.

### Acknowledgments

K. T. Y. and S. R. contributed equally to this work. We acknowledge T. Toonen and C. Berkhout for the continuous technical supports, and J. Mentink for fruitful discussions. We are grateful for computational support from the University of York High-Performance Computing service, VIKING and the Research Computing team. This work was partly supported by the European Research Council Grant Agreement No.856538 (3D-MAGiC), by the FOM programme Exciting Exchange, de Nederlandse Organisatie voor Wetenschappelijk Onderzoek (NWO), by the EU H2020 Program Grant Agreement No. 713481 (SPICE) and No. 737093 (FEMTOTERABYTE), by JSPS KAKENHI No. 24K00938, No. 22K14588, No. 15H05702, No. 20H00332, No. 20H05665, No. 17J07326, and No. 18J22219, and by the Collaborative Research Program of the Institute for Chemical Research, Kyoto University.

### REFERENCES

1. S. Chikazumi, “*Physics of Magnetism*,” International Series of Monographs on Physics, Oxford University Press, USA, ed. 2, 2009.
2. I. M. Miron et al., “Perpendicular switching of a single ferromagnetic layer induced by in-plane current injection,” *Nature* vol. 476, pp. 189–193, 2011, doi: [10.1038/nature10309](https://doi.org/10.1038/nature10309)
3. L. Liu, C.-F. Pai, Y. Li, H. W. Tseng, D. C. Ralph, and R. A. Buhrman, “Spin-Torque Switching with the Giant Spin Hall Effect of Tantalum,” *Science* vol. 336, pp. 555–558, 2012, doi: [10.1126/science.1218197](https://doi.org/10.1126/science.1218197).
4. Y. Shiota, T. Nozaki, F. Bonell, S. Murakami, T. Shinjo, and Y. Suzuki, “Induction of coherent magnetization switching in a few atomic layers of FeCo using voltage pulses,” *Nat. Mater.* vol. 11, pp. 39–43, 2012, doi: [10.1038/nmat3172](https://doi.org/10.1038/nmat3172).
5. S. Kanai, M. Yamanouchi, S. Ikeda, Y. Nakatani, F. Matsukura, and H. Ohno, “Electric field-induced magnetization reversal in a perpendicular-anisotropy CoFeB-MgO magnetic tunnel junction,” *Appl. Phys. Lett.* vol. 101, Art. no. 122403, 2012, doi: [10.1063/1.4753816](https://doi.org/10.1063/1.4753816).
6. M. H. Kryder et al., “Heat Assisted Magnetic Recording,” *Proc. IEEE* vol. 96, pp. 1810–1835, 2008, doi: [10.1109/JPROC.2008.2004315](https://doi.org/10.1109/JPROC.2008.2004315).
7. J. G. Zhu, X. C., Zhu, and Y. H. Tang, “Microwave Assisted Magnetic Recording,” *IEEE Trans. Magn.* vol. 44, pp. 125–131, 2007, doi: [10.1109/TMAG.2007.911031](https://doi.org/10.1109/TMAG.2007.911031)
8. D. Apalkov, B. Dieny, and J. M. Slaughter, “Magnetoresistive Random Access Memory,” *IEEE Proc.* vol. 104, pp. 1796–1830, 2006, doi: [10.1109/JPROC.2016.2590142](https://doi.org/10.1109/JPROC.2016.2590142).
9. K. Garello, C. O. Avci, I. M. Miron, M. Baumgartner, A. Ghosh, S. Auffret, O. Boulle, G. Gaudin, and P. Gambardella, “Ultrafast magnetization switching by spin-orbit torques,” *Appl. Phys. Lett.* vol. 105, Art. no. 212402, 2014, doi: [10.1063/1.4902443](https://doi.org/10.1063/1.4902443).
10. B. Dieny et al., “Opportunities and challenges for spintronics in the microelectronics industry,” *Nat. Electron.* vol. 3, pp. 446–459, 2020, doi: [10.1038/s41928-020-0461-5](https://doi.org/10.1038/s41928-020-0461-5).
11. C. H. Back et al., “Magnetization Reversal in Ultrashort Magnetic Field Pulses,” *Phys. Rev. Lett.* vol. 81, Art. no. 3251, 1998, doi: [10.1103/PhysRevLett.81.3251](https://doi.org/10.1103/PhysRevLett.81.3251).
12. C. H. Back, et al., “Minimum Field Strength in Precessional Magnetization Reversal,” *Science* vol. 285, pp. 864–867, 1999, doi: [10.1126/science.285.5429.864](https://doi.org/10.1126/science.285.5429.864).
13. Th. Gerrits, H. A. M. van den Berg, J. Hohlfield, L. Bar, Th. Rasing, “Ultrafast precessional magnetization reversal by picosecond magnetic field pulse shaping,” *Nature* vol. 418, pp. 509–512, 2002, doi: [10.1038/nature00905](https://doi.org/10.1038/nature00905).
14. I. Tudosa et al., “The ultimate speed of magnetic switching in granular recording media,” *Nature* vol. 428, pp. 831–833, 2004, doi: [10.1038/nature00905](https://doi.org/10.1038/nature00905).
15. S. K. Kim, G. S. D. Beach, K.-J. Lee, T. Ono, Th. Rasing, and H. Yang, Ferrimagnetic spintronics, “Ferrimagnetic spintronics,” *Nat. Mater.* vol. 21, pp. 24–34, 2022, doi: [10.1038/s41563-021-01139-4](https://doi.org/10.1038/s41563-021-01139-4).
16. T. Jungwirth, X. Marti, P. Wadley, and J. Wunderlich, “Antiferromagnetic spintronics,” *Nat. Nanotechnol.* vol. 11, pp. 231–241, 2016, doi: [10.1038/nnano.2016.18](https://doi.org/10.1038/nnano.2016.18).
17. T. N emec, M. Fiebig, T. Kampfrath, and A. V. Kimel, “Antiferromagnetic opto-spintronics,” *Nat. Phys.* vol. 14, pp. 229–241, 2018, doi: [10.1038/s41567-018-0051-x](https://doi.org/10.1038/s41567-018-0051-x).
18. E. Beaurepaire, J.-C. Merle, A. Daunois, and J.-Y. Bigot, “Ultrafast Spin Dynamics in Ferromagnetic Nickel,” *Phys. Rev. Lett.* vol. 76, Art. no. 4250, 1994, doi: [10.1103/PhysRevLett.76.4250](https://doi.org/10.1103/PhysRevLett.76.4250).
19. A. V. Kimel, and M. Li, “Writing magnetic memory with ultrashort light pulses,” *Nat. Rev. Mater.* vol. 4, pp.189–200, 2019, doi: [10.1038/s41578-019-0086-3](https://doi.org/10.1038/s41578-019-0086-3).
20. C. D. Stanciu et al., “All-optical magnetic recording with circularly polarized light,” *Phys. Rev. Lett.* vol. 99, Art. no. 047601, 2007, doi: [10.1103/PhysRevLett.99.047601](https://doi.org/10.1103/PhysRevLett.99.047601).
21. K. Vahaplar et al., “Ultrafast path for optical magnetization reversal via a strongly nonequilibrium state,” *Phys. Rev. Lett.* vol. 103, Art. no. 117201, 2009, doi: [10.1103/PhysRevLett.103.117201](https://doi.org/10.1103/PhysRevLett.103.117201).
22. I. Radu et al., “Transient ferromagnetic-like state mediating ultrafast reversal of antiferromagnetically coupled spins,” *Nature* vol. 472, 205–208, 2011, doi: [10.1038/nature09901](https://doi.org/10.1038/nature09901).
23. T. A. Ostler et al., “Ultrafast heating as a sufficient stimulus for magnetization reversal in a ferrimagnet,” *Nat. Commun.* vol. 3, Art. no. 666, 2012, doi: [10.1038/ncomms1666](https://doi.org/10.1038/ncomms1666).
24. A. R. Khorsand et al., “Role of magnetic circular dichroism in all-optical magnetic recording,” *Phys. Rev. Lett.* vol. 108, 127205, 2012, doi: [10.1103/PhysRevLett.108.057202](https://doi.org/10.1103/PhysRevLett.108.057202).
25. S. Iihama et al., “Single-Shot Multi-Level All-Optical Magnetization Switching Mediated by Spin Transport,” *Adv. Mater.* vol. 30, Art. no. 1804004, 2018, doi: [10.1002/adma.201804004](https://doi.org/10.1002/adma.201804004).
26. Q. Remy et al., “Energy Efficient Control of Ultrafast Spin Current to Induce Single Femtosecond Pulse Switching of a Ferromagnet,” *Adv. Sci.* vol. 7, Art. no. 2001996, 2020, doi: [10.1002/adv.202001996](https://doi.org/10.1002/adv.202001996).
27. C.-H. Lambert et al., “All-optical control of ferromagnetic thin films and nanostructures,” *Science* vol. 345, pp.1337–1340, 2014, doi: [10.1126/science.1253493](https://doi.org/10.1126/science.1253493).
28. M. S. El Hadri et al., “Two types of all-optical magnetization switching mechanisms using femtosecond laser pulses,” *Phys. Rev. B* vol. 94, Art. no. 064412, 2016, doi: [10.1103/PhysRevB.94.064412](https://doi.org/10.1103/PhysRevB.94.064412).
29. M. S. El Hadri et al., “Domain size criterion for the observation of all-optical helicity-dependent switching in magnetic thin films,” *Phys. Rev. B* vol. 94, Art. no. 064419, 2016, doi: [10.1103/PhysRevB.94.064419](https://doi.org/10.1103/PhysRevB.94.064419).
30. R. Medapalli et al., “Multiscale dynamics of helicity-dependent all-optical magnetization reversal in ferromagnetic Co/Pt multilayers,” *Phys. Rev. B* vol. 96, Art. no. 224421, 2017, doi: [10.1103/PhysRevB.96.224421](https://doi.org/10.1103/PhysRevB.96.224421).
31. Y. Quessab et al., “Helicity-dependent all-optical domain wall motion in ferromagnetic thin films,” *Phys. Rev. B* vol. 97, Art. no. 054419, 2018, doi: [10.1103/PhysRevB.97.054419](https://doi.org/10.1103/PhysRevB.97.054419).
32. U. Parlak, R. Adam, D. E. B urgler, S. Gang, and C. M. Schneider, “Optically induced magnetization reversal in [Co/Pt]<sub>N</sub> multilayers: Role of domain wall dynamics,” *Phys. Rev. B* vol. 98, Art. no. 214443, 2018, doi: [10.1103/PhysRevB.98.214443](https://doi.org/10.1103/PhysRevB.98.214443).
33. G. Kichin, M. Hehn, J. Gorchon, G. Malinowski, J. Hohlfield, and S. Mangin, “From Multiple- to Single-Pulse All-Optical Helicity-Dependent Switching in Ferromagnetic Co/Pt Multilayers,” *Phys. Rev. Appl.* vol. 12, Art. no. 024019, 2019, doi: [10.1103/PhysRevApplied.12.024019](https://doi.org/10.1103/PhysRevApplied.12.024019).
34. F. Cheng et al., “All-Optical Helicity-Dependent Switching in Hybrid Metal–Ferromagnet Thin Films,” *Adv. Opt. Mater.* vol. 8, Art. no. 2000379, 2020, doi: [10.1002/adom.202000379](https://doi.org/10.1002/adom.202000379).
35. Y. K. Takahashi et al., “Accumulative Magnetic Switching of Ultrahigh-Density Recording Media by Circularly Polarized Light,” *Phys. Rev. Appl.* vol. 6, Art. no. 054004, 2016, doi: [10.1103/PhysRevApplied.6.054004](https://doi.org/10.1103/PhysRevApplied.6.054004).
36. R. John et al., “Magnetisation switching of FePt nanoparticle recording medium by femtosecond laser pulses,” *Sci. Rep.* vol. 7, Art. no. 4114, 2017, doi: [10.1038/s41598-017-04167-w](https://doi.org/10.1038/s41598-017-04167-w).

38. J. Gorchon, Y. Yang, and J. Bokor, "Model for multishot all-thermal all-optical switching in ferromagnets," *Phys. Rev. B* vol. 94, Art. no. 020409, 2016, doi: [10.1103/PhysRevB.94.020409](https://doi.org/10.1103/PhysRevB.94.020409).
39. M. O. A. Ellis, E. E. Fullerton, and R. W. Chantrell, "All-optical switching in granular ferromagnets caused by magnetic circular dichroism," *Sci Rep.* vol. 6, Art. no. 30522, 2016, doi: [10.1038/srep30522](https://doi.org/10.1038/srep30522).
40. K. T. Yamada et al., "Magnetization reversal of a ferromagnetic Pt/Co/Pt film by helicity dependent absorption of visible to near-infrared laser pulses," (Preprint) [arXiv:2201.01141](https://arxiv.org/abs/2201.01141), v1, submitted: Jan 2022.
41. K. T. Yamada et al., "Efficient All-Optical Helicity Dependent Switching of Spins in a Pt/Co/Pt Film by a Dual-Pulse Excitation," *Front. Nanotechnol.* vol. 4, Art. no. 765848, 2022, doi: [10.3389/fnano.2022.765848](https://doi.org/10.3389/fnano.2022.765848).
42. S. Alebrand, A. Hassdenteufel, D. Steil, M. Cinchetti, and A. Aeschlimann, "Interplay of heating and helicity in all-optical magnetization switching," *Phys. Rev. B* vol. 85, Art. no. 092401, 2012, doi: [10.1088/0953-8984/26/10/103202](https://doi.org/10.1088/0953-8984/26/10/103202).
43. R. F. L. Evans, W. J. Fan, P. Chureemart, T. A. Ostler, M. O. A. Ellis, and R. W. Chantrell, "Atomistic spin model simulations of magnetic nanomaterials," *J. Phys.: Condens. Matter* vol. 26, Art. no. 103202, 2014, doi: [10.1088/0953-8984/26/10/103202](https://doi.org/10.1088/0953-8984/26/10/103202).
44. E. Iacocca et al., "Spin-current-mediated rapid magnon localisation and coalescence after ultrafast optical pumping of ferrimagnetic alloys," *Nat. Commun.* vol. 10, Art no. 1756, 2019, doi: [10.1038/s41467-019-09577-0](https://doi.org/10.1038/s41467-019-09577-0).
45. B. Pfau et al., "Ultrafast optical demagnetization manipulates nanoscale spin structure in domain walls," *Nat. Commun.* vol. 3, Art. no. 1100, 2012, doi: [10.1038/ncomms2108](https://doi.org/10.1038/ncomms2108).
46. S. Yoshida et al., "Probing ultrafast spin dynamics with optical pump-probe scanning tunnelling microscopy," *Nat. Nanotechnol.* vol. 9, pp. 588–593, 2014, doi: [10.1038/nnano.2014.125](https://doi.org/10.1038/nnano.2014.125).
47. A. Nordrum, "The fight for the future of the disk drive," *IEEE Spectrum* vol. 56, pp. 44–47, 2019, doi: [10.1109/MSPEC.2019.8594796](https://doi.org/10.1109/MSPEC.2019.8594796).
48. T. Shima, K. Takahashi, Y. K. Takahashi, and K. Hono, "Preparation and magnetic properties of highly coercive FePt films," *Appl. Phys. Lett.* vol. 81, Art. no. 1050, 2022, doi: [10.1063/1.498504](https://doi.org/10.1063/1.498504).
49. A. L. Sukstanskii, and K. I. Primak, "Domain structure in an ultrathin ferromagnetic film," *J. Magn. Magn. Mater.* vol. 169, pp. 31–38, 1997, doi: [10.1016/S0304-8853\(96\)00729-9](https://doi.org/10.1016/S0304-8853(96)00729-9).
50. J. M. Liu, "Simple technique for measurements of pulsed Gaussian-beam spot sizes," *Opt. Lett.* vol. 7, pp. 196–198, 1982, doi: [10.1364/OL.7.000196](https://doi.org/10.1364/OL.7.000196).
51. R. Moreno, R. F. L. Evans, S. Khmelevskiy, M. C. Muñoz, R. W. Chantrell, and O. Chubykalo-Fesenko, "Temperature-dependent exchange stiffness and domain wall width in Co," *Phys. Rev. B* vol. 94, Art. no. 104433, 2016, doi: [10.1103/PhysRevB.94.104433](https://doi.org/10.1103/PhysRevB.94.104433).
52. L. Jiang, and H.-L. Tsai, "Improved Two-Temperature Model and Its Application in Ultrashort Laser Heating of Metal Films," *J. Heat Transfer.* vol. 127, pp. 1167–1173, 2005, doi: [10.1115/1.2035113](https://doi.org/10.1115/1.2035113).